Eur. Phys. J. AP **20**, 145–150 (2002)
DOI: 10.1051/epjap:2002085

THE EUROPEAN PHYSICAL JOURNAL
APPLIED PHYSICS

The distributed sources method: a concept for open magnetic cores modelling*

N. Liebeaux[a] and D. Placko[b]

École Normale Supérieure de Cachan, Laboratoire d'Électricité, Signaux & Robotique (LESiR), 61 avenue du Président Wilson, 94235 Cachan Cedex, France

Received: 19 July 2001 / Received in final form: 27 June 2002 / Accepted: 28 June 2002
Published online: 25 October 2002 –

Abstract. This paper presents a original method for open magnetic cores modelling. It is called the distributed point source method. It is based on a spatial distribution of point sources located on the core surfaces emitting the magnetic flux, called the active surfaces. Compared to Finite Elements methods, the DSPM method requires only the meshing of these active surfaces, which considerably reduces the solving process time. In this paper, the DSPM method is applied on a magnetic cylindrical core, placed in free space.

PACS. 81.70.Ex Nondestructive testing: electromagnetic testing, eddy-current testing – 85.70.Ay Magnetic device characterization, design, and modeling

1 Introduction

For electromagnetic modelling problems, numerical simulations, such as finite elements methods (FEM) for instance, are widely used. Exact analytical solutions exist only for very simple geometries which don't always fit to realistic cases. For example, various configurations consisting in a sensor located in front of a target are encountered in Non Destructive Evaluation (NDE), but solutions exist only for a limited number of particular geometries of sensors and targets, as it has been demonstrated in [3]. On other hand, the use of numerical methods combined with the ever increasing power of modern computers, leads to the capacity of solving almost any kind of problem. But it becomes obvious that 3D complex geometries require important computation time. Furthermore, these softwares are not easy-to-use, and require users' knowledge of physical phenomena and solving algorithms. Thus, it is evident that a quick and efficient numerical method could be of some interest if its design makes it quicker and easier to handle in comparison to the FEM. This paper proposes an original numerical method, called DPSM for Distributed Point Source Method, which can be used to calculate magnetic potentials and fields. As it will be detailed in Section 2, the method is based on the use of point sources that cover all closed surfaces involved in the problem definition, and applied in the area of this paper for solving problems of open magnetic cores.

* This paper has been first presented orally at the C2I colloquium in February 2001

[a] e-mail: nicolas.liebeaux@lesir.ens-cachan.fr
[b] e-mail: dominique.placko@lesir.ens-cachan.fr

2 The distributed point sources method (DPSM)

2.1 Introduction

Magnetic fields emitted by open magnetic cores (electrical motors, magnetic and eddy current sensors) are modeled in this section. Solving such problems without any approximations would be very difficult, as we can see through some approaches in this domain of electromagnetic modelling [1,2,4–6]. A open magnetic core (see Sect. 3 The Geometry) is considered for the illustrative example.

The basic principle of the DPSM is sketched in Figure 1. The implementation of the model simply requires discretization of the active surfaces of the core to obtain an array of point sources, so that the initial complexity is changed into a superposition of elementary problems. The active surfaces of the core are discretized into a finite number of elementary surfaces dS, a point source being placed at the centroid of every elemental surface. It is interesting to note that the energy (or the power) radiated by such a system is the product of a scalar quantity and the flux of a vector (or the time derivative of the flux, for power). Let us denote the scalar quantity by θ_k, and φ_k the flux emitted by the source k. In the application described in this paper, θ_k and φ_k represent the magnetic scalar potential and the flux of magnetic induction, respectively. As an example, Figure 1 presents an active surface that have been discretized into surface elements dS. It also shows that because of rotating symmetry, the real elemental surface dS can be changed into a hemispherical surface dS with radius r ($dS = 2\pi\, r^2$).

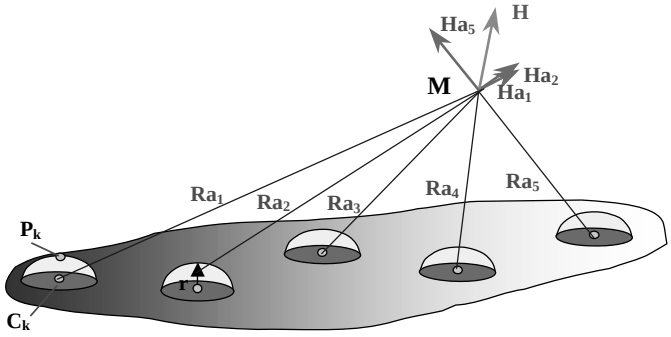

Fig. 1. Discretization of the core surface into a finite number of hemispherical sources.

2.2 Boundary conditions

One needs to introduce the boundary conditions before solving the problem. For computing the values of the flux φ_k for N sources one needs a number of N equations. These equations are obtained by introducing boundary conditions on the scalar quantity φ_k at N given points. Our choice was to place these specific points at the apex of the hemispherical surfaces (then r is normal to the surface). These specific points are labelled P_k in Figure 1. Clearly, the greater the number of points, the smaller the value of radius r. Hence, when N tends to infinity, r tends to 0 and P_k points tend to reach the surface of the core, *i.e.* P_k points reach center points C_k.

In [5,6], the DPSM method was applied on two closed surfaces standing for the North and South poles of a U-shaped sensor. In that configuration, the magnetic scalar potentials $\theta_{\text{south pole}}$ and $\theta_{\text{north pole}}$ were assumed to be constants. In this application, the potential θ is not constant, as it will be explained in Section 3. That is why the color of the active surface in Figure 1 is black and white gradually shaded: one potential value is assigned to each point source on the active surface.

The active surfaces are discretized into elementary surfaces dS. At the center C_k of the k-th elemental surface dS a point source emitting a flux φ_k is placed. From the conservation of the magnetic flux, one can write that the summation of the flux emitted by all point sources is equal to zero,

$$\varphi = \sum_{\text{active surface}} \varphi_{\mathrm{C}_k} = 0. \tag{1}$$

The magnetic potential at a given point M in the space is obtained by considering the contribution of all magnetic point sources:

$$\theta = \sum_{\text{active surface}} \theta_{\mathrm{C}_k}. \tag{2}$$

General relations between the magnetic field and the magnetic scalar potential are given by:

$$\mathbf{H} = -\frac{1}{\mu}\frac{\mathrm{d}\theta}{\mathrm{d}\mathbf{R}} \text{ and } \varphi = \int\int \mu_0 \mathbf{H}\cdot\mathbf{dS}. \tag{3}$$

It yields in our case, for the k-th point source:

$$H_k = \frac{\varphi_k}{2\pi\mu_0 R^2} \text{ and } \theta_k = \frac{\varphi_k}{2\pi\mu_0 R}\cdot \tag{4}$$

2.3 Solutions of coupling equations

At this step, the value of the magnetic flux emitted by the point sources is unknown. An additional boundary condition is then introduced to obtain a new equation set. This is done by computing the magnetic potential θ_k at each peak point P_k of hemispherical surface (radius r), due to all sources C_i:
θ_k can be obtained from:

$$\theta_k = \sum_{\text{all sources}} \varphi_{C_i} * f(P_k - C_i) \text{ where } f(R) = \frac{1}{2\pi\mu_0 R}\cdot \tag{5}$$

Considering an example where the active surface has five hemispherical surfaces (see Fig. 1), the lower disk has two surfaces, and the cylinder has one, we have:

$$\begin{pmatrix}\theta_{P_1}\\ \theta_{P_2}\\ \theta_{P_3}\\ \theta_{P_4}\\ \theta_{P_5}\end{pmatrix} = \begin{bmatrix}F_{P_1C_1} & F_{P_1C_2} & F_{P_1C_3} & F_{P_1C_4} & F_{P_1C_5}\\ F_{P_2C_1} & F_{P_2C_2} & F_{P_2C_3} & F_{P_2C_4} & F_{P_2C_5}\\ F_{P_3C_1} & F_{P_3C_2} & F_{P_3C_3} & F_{P_3C_4} & F_{P_3C_5}\\ F_{P_4C_1} & F_{P_4C_2} & F_{P_4C_3} & F_{P_4C_4} & F_{P_4C_5}\\ F_{P_5C_1} & F_{P_5C_2} & F_{P_5C_3} & F_{P_5C_4} & F_{P_5C_5}\end{bmatrix} * \begin{pmatrix}\varphi_{C_1}\\ \varphi_{C_2}\\ \varphi_{C_3}\\ \varphi_{C_4}\\ \varphi_{C_5}\end{pmatrix}\cdot \tag{6}$$

So that:

$$\Theta = F * \Psi. \tag{7}$$

Inversion of equation (7) gives the magnetic flux for all point sources:

$$\Psi = F^{-1}\Theta = G\,\Theta \tag{8}$$

which gives:

$$\Psi = \begin{pmatrix}\varphi_{C_1}\\ \varphi_{C_2}\\ \varphi_{C_3}\\ \varphi_{C_4}\\ \varphi_{C_5}\end{pmatrix} = \begin{bmatrix}G_{P_1C_1} & G_{P_1C_2} & G_{P_1C_3} & G_{P_1C_4} & G_{P_1C_5}\\ G_{P_2C_1} & G_{P_2C_2} & G_{P_2C_3} & G_{P_2C_4} & G_{P_2C_5}\\ G_{P_3C_1} & G_{P_3C_2} & G_{P_3C_3} & G_{P_3C_4} & G_{P_3C_5}\\ G_{P_4C_1} & G_{P_4C_2} & G_{P_4C_3} & G_{P_4C_4} & G_{P_4C_5}\\ G_{P_5C_1} & G_{P_5C_2} & G_{P_5C_3} & G_{P_5C_4} & G_{P_5C_5}\end{bmatrix} * \begin{pmatrix}\theta_{P_1}\\ \theta_{P_2}\\ \theta_{P_3}\\ \theta_{P_4}\\ \theta_{P_5}\end{pmatrix}. \tag{9}$$

The condition on the flux (Eq. (1)) in combination with equation (9) gives a new equation to determine the values of θ_{P_i}:

$$\varphi_C = \sum_i \theta_{P_i} \sum_j G_{P_iC_j} = 0. \tag{10}$$

Knowing the magnetic flux values, the magnetic potential or the field in the space around the core is computed from equations (3, 6).

Let us now apply this technique to model the magnetic field generated by a magnetic open core consisting in a bar with infinite magnetic permeability.

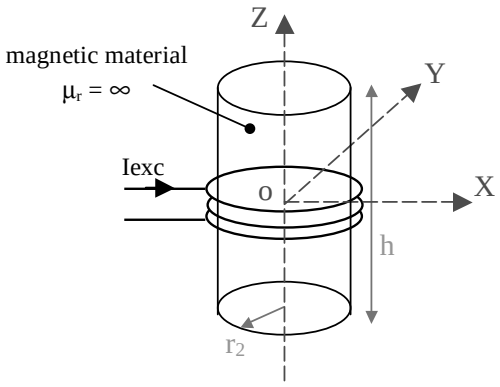

Fig. 2. Geometry under test.

3 The geometry

The geometry studied in this paper is a small magnetic bar, with infinite magnetic permeability ($\mu_r = \infty$), as described in Figure 2.

The radius r_2 is 4 mm long, and the height h is 3 cm. A current density of 1 A/m^2 is applied between radii r_2 and $r = 5$ mm, and between heights $-h/6$ and $+h/6$ – a third of the total height.

4 DPSM formulation and results

4.1 DPSM formulation applied to the magnetic bar

In part 2, general principles of the DPSM method have been presented. It is now applied in order to model the magnetic bar shown in Figure 2. The bar can be divided into three closed active surfaces: the upper disk, the lower disk, and the cylindrical surface. We have placed $N = 500$ point sources, which have been equally spaced on the three closed surfaces of the bar.

The boundary conditions applied are the following:

- the upper disk point sources potential θ_U is set to $\alpha = +0.5$ A. The same condition is applied on the point sources located on the upper one-third of the cylinder;
- the lower disk point sources potential θ_L is set to $-\beta = -0.5$ A. The same condition is applied on the point sources located on the lower one-third of the cylinder;
- the point sources located between $+h/6$ and $-h/6$ (the middle of the cylinder where current density excitation is applied) are characterized by their potential $\theta_C(z) = \gamma(z)$ gradually increasing from +0.5 A to −0.5 A, in order to take into account the real excitation conditions due to the excitation windings.

These boundary conditions are shown in Figure 3.

If we consider one point source on each lower disk (L) and upper disk (U), and three point sources on the cylinder surface (C), equation (6) can be rewritten as below, with p suffix for peak, and c suffix for center:

$$\begin{pmatrix}\theta_{Up_1}\\ \theta_{Lp_1}\\ \theta_{Cp_1}\\ \theta_{Cp_2}\\ \theta_{Cp_3}\end{pmatrix} = \begin{pmatrix}+\alpha\\ -\beta\\ +\gamma\\ +\gamma\\ +\gamma\end{pmatrix}$$
$$= \begin{bmatrix} F_{Up_1Uc_1} & F_{Up_1Lc_1} & F_{Up_1Cc_1} & F_{Up_1Cc_2} & F_{Up_1Cc_3}\\ F_{Lp_1Uc_1} & F_{Lp_1Lc_1} & F_{Lp_1Cc_1} & F_{Lp_1Cc_2} & F_{Lp_1Cc_3}\\ F_{Cp_1Uc_1} & F_{Cp_1Lc_1} & F_{Cp_1Cc_1} & F_{Cp_1Cc_2} & F_{Cp_1Cc_3}\\ F_{Cp_2Uc_1} & F_{Cp_2Lc_1} & F_{Cp_2Cc_1} & F_{Cp_2Cc_2} & F_{Cp_2Cc_3}\\ F_{Cp_2Uc_1} & F_{Cp_3Lc_1} & F_{Cp_3Cc_1} & F_{Cp_3Cc_2} & F_{Cp_3Cc_3}\end{bmatrix} * \begin{pmatrix}\varphi_{U_{c_1}}\\ \varphi_{L_{c_1}}\\ \varphi_{C_{c_1}}\\ \varphi_{C_{c_2}}\\ \varphi_{C_{c_3}}\end{pmatrix}. \quad (11)$$

This system of equations with nine sub matrices can be rewritten as:

$$\begin{aligned}\Theta_U &= F_{UU} \star \Psi_U + F_{UL} \star \Psi_L + F_{UC} * \Psi_C\\ \Theta_L &= F_{LU} \star \Psi_U + F_{LL} \star \Psi_L + F_{LC} * \Psi_C\\ \Theta_C &= F_{CU} \star \Psi_U + F_{CL} \star \Psi_L + F_{CC} * \Psi_C. \end{aligned} \quad (12)$$

Inversion of equation (8) leads to the expressions of φ_i.

$$\Psi = \begin{pmatrix}\varphi_{Uc_1}\\ \varphi_{Lc_1}\\ \varphi_{Cc_1}\\ \varphi_{Cc_2}\\ \varphi_{Cc_3}\end{pmatrix}$$
$$== \begin{bmatrix} G_{Up_1Uc_1} & G_{Up_1Lc_1} & G_{Up_1Cc_1} & G_{Up_1Cc_2} & G_{Up_1Cc_3}\\ G_{Lp_1Uc_1} & G_{Lp_1Lc_1} & G_{Lp_1Cc_1} & G_{Lp_1Cc_2} & G_{Lp_1Cc_3}\\ G_{Cp_1Uc_1} & G_{Cp_1Lc_1} & G_{Cp_1Cc_1} & G_{Cp_1Cc_2} & G_{Cp_1Cc_3}\\ G_{Cp_2Uc_1} & G_{Cp_2Lc_1} & G_{Cp_2Cc_1} & G_{Cp_2Cc_2} & G_{Cp_2Cc_3}\\ G_{Cp_3Uc_1} & G_{Cp_3Lc_1} & G_{Cp_3Cc_1} & G_{Cp_3Cc_2} & G_{Cp_3Cc_3}\end{bmatrix} * \begin{pmatrix}+\alpha\\ -\beta\\ +\gamma\\ +\gamma\\ +\gamma\end{pmatrix}. \quad (13)$$

The condition on the flux (Eq. (1)) in combination with equation (13) gives a new equation to determine the values of α, β, and $\gamma(z)$:

$$\varphi_U + \varphi_L + \varphi_C = \alpha \sum_{i,j} G_{ij} - \beta \sum_{k,j} H_{kl} + \gamma \sum_{m,n} I_{mn} = 0. \quad (14)$$

4.2 Results

Figure 4 shows the magnetic scalar potential θ outside the bar, where x varies from r_2 to $3r_2$, and z from $-h/2$ to $+h/2$. The decrease of θ is noticeable, for large values of x, limiting value of θ is 0 for infinite x. On the cylinder surface, two equal steps, with a linear decrease joining them, stand for the boundary condition applied on θ, on the point sources located on the outside cylinder surface.

5 Finite element simulation - comparisons

The geometry has been studied using ANSYS finite element (FE) software [7], in order to compare the results. Three positions are then examined.

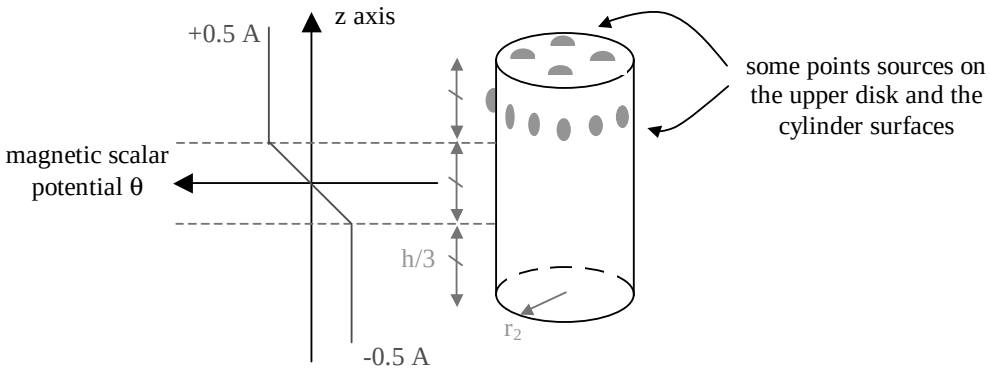

Fig. 3. Magnetic scalar potential boundary conditions.

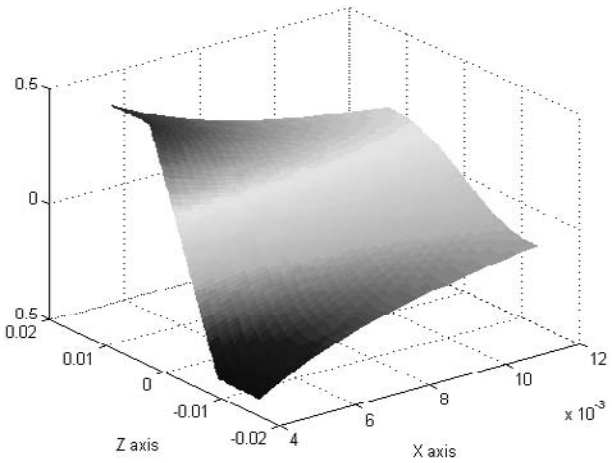

Fig. 4. Magnetic scalar potential θ outside the bar.

5.1 Position 1

Position 1 is along the symmetry axis. Obviously, H_x and H_y components are null because of symmetry. ANSYS results are plotted with lines, and DPSM simulation by crosses.

The graph (Fig. 5) shows good match between the two simulations. The average error never exceeds 2 A/m. As expected, with infinite magnetic permeability μ_r, induction field H is null. As soon as the height z gets close to $+h/2$ or $-h/2$ *i.e.* ± 1.5 cm - the point where H is calculated is nearer to the point sources located on the upper/lower disks. It means that the distance R (see Eq. (4)) is becoming smaller, H field gets closer to infinity.

5.2 Position 2

Position 2 is along an axis parallel to z axis, for a radius value of $r = r_2 + 1$ mm. Figures 6 and 7 represent components H_x and H_z for this radius. Average errors are respectively 1.5 A/m and 2.23 A/m, the DPSM curves fitting the FE simulated curves.

5.3 Position 3

Position 3 is obtained for $z = 0$. H_x and H_y component are zero, the only existing component is the z component, shown in Figure 8. Average error is 0.7 A/m.

It is interesting to notice that DPSM model gives higher values around the position $z = 5$ mm. This is precisely an area where the DPSM mesh is not sufficient enough to produce accurate results, because of the radius value of the hemispherical source. The cylinder point sources are located on the outside cylinder surface, with a radius value of 0.54 mm. Equation (4) clearly demonstrates that the point source and the apex must not be the same. Since that ANSYS positions are used in the DPSM model to get a realistic comparison, the points in the area $x = 5$ mm are too close to the point sources, which gives higher values of field and magnetic scalar potential than in the FE simulation.

6 Conclusion

The DPSM model has been used to calculate the magnetic scalar potential θ and the induction field H created by a magnetic bar. Substitution of point sources array for the transducer closed active surface (in this case the magnetic core with its winding) allows to synthesize easily a reliable value of θ and H in the whole surrounding space, because the initial complex case is changed into a limited number of quite simple problems. It has been demonstrated that this original modelling shows good accuracy, compared to finite element simulation. The DPSM method is efficient and quicker, because only active surface needs to be meshed. Finite elements methods require the meshing of all the area – or volume – under test, and can lead to time-consuming simulations in the case of complex geometries. In our case, as soon as closed surfaces with proper boundary conditions can be defined, the method can be applied. The results are obtained no matter how complex the geometry is: the only time-consuming operation lies in the inversion of matrix F, as defined in equations (7, 8). So, interesting results can be obtained very fast as soon as closed surfaces are roughly meshed, when no high precision is needed.

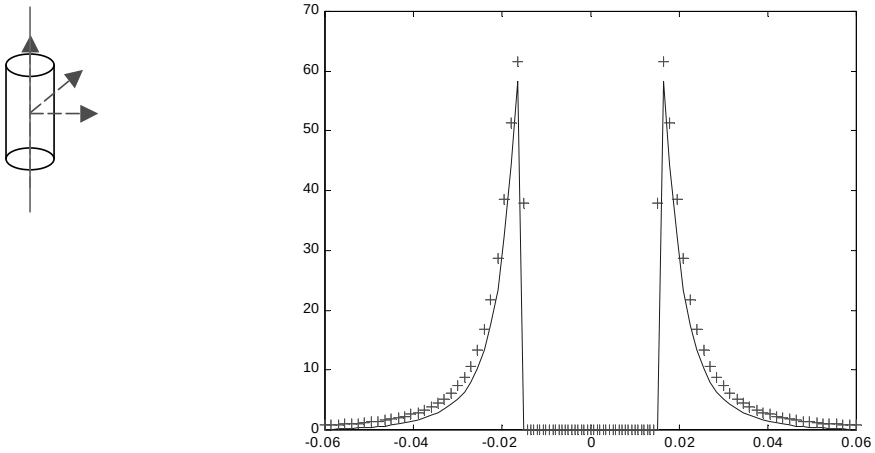

Fig. 5. H_z component as a function of height z (position 1).

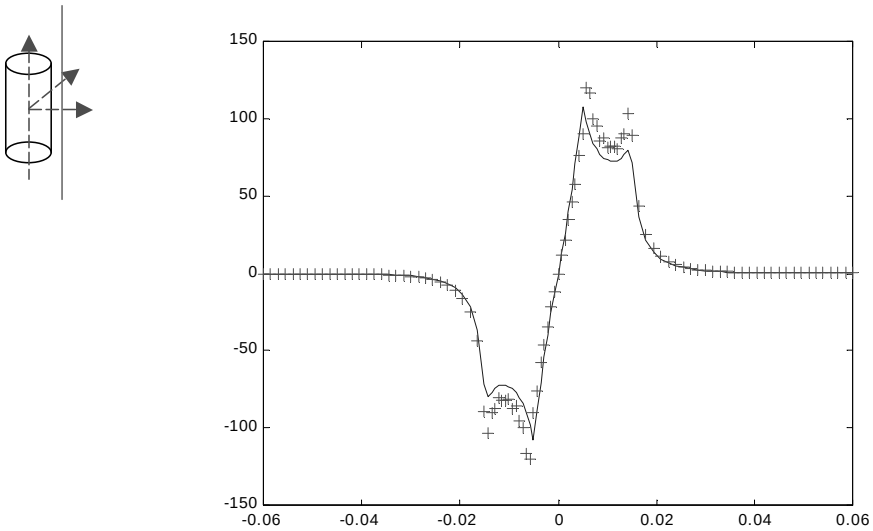

Fig. 6. H_x component of the induction field H as a function of height z (position 2).

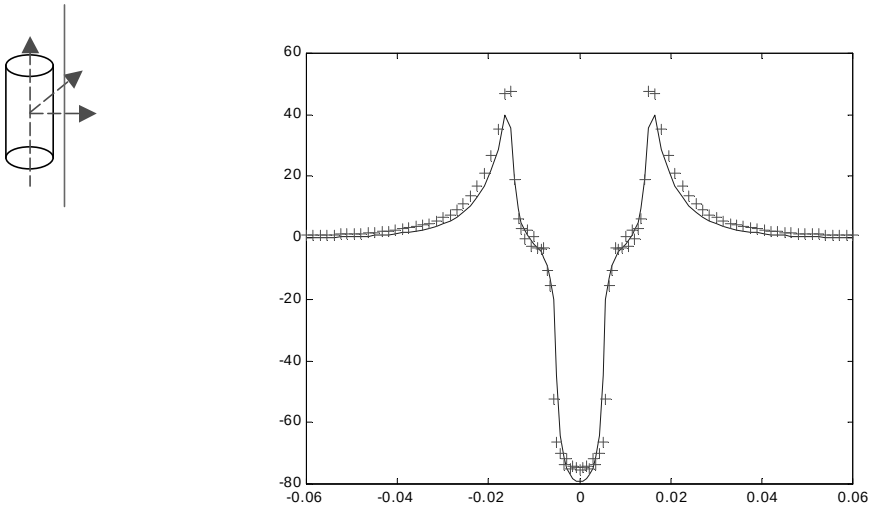

Fig. 7. H_z component of the induction field H as a function of height z (position 2).

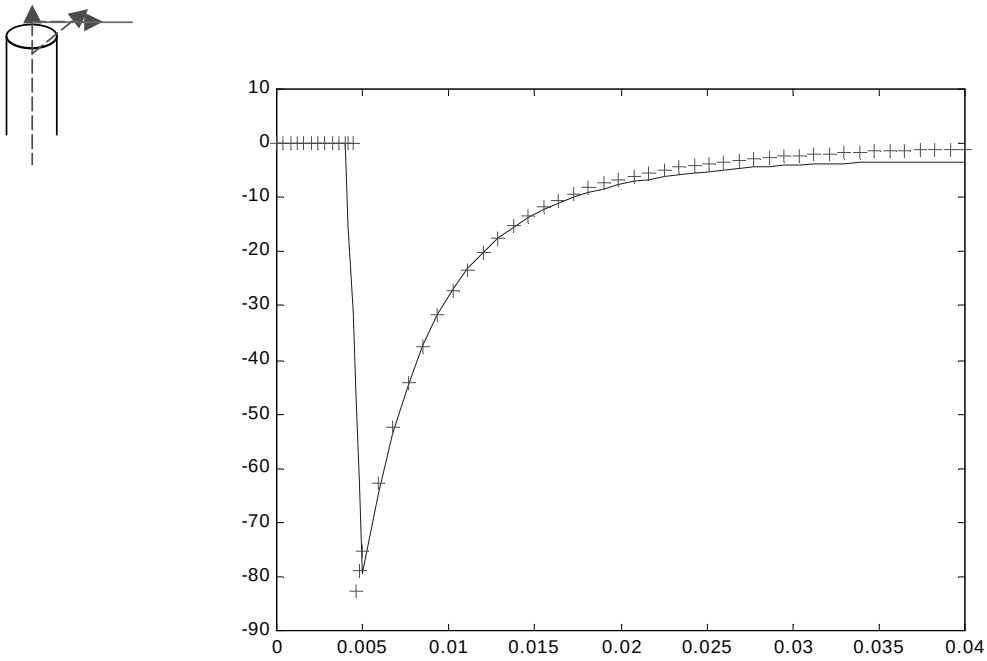

Fig. 8. H_z component of the induction field H along the x axis (position 3).

Furthermore, this method is closer to the electromagnetic phenomena involved, and leads to a better understanding of the problem, because no harsh algorithms are involved. Even if the method probably will not cover every targets and sensors configurations, it presents a few advantages and can be seen as a powerful tool in NDE, mainly in terms of generic formulation, since it works also for ultrasonic problems [6], for example.

References

1. N. Hartfield, J.R. Bowler, Proc. Res. Soc. London A **453**, 1121 (1997)
2. N. Ida, Computer modelling of eddy current fields, *Nondestructive testing handbook, Vol. 4, Electromagnetic testing*, 2nd edn., edited by P. McIntire, M.L. Mester (American society for nondestructive testing, Inc., Columbus, OH, 1986), pp. 561–590
3. J.R. Bowler, H.A. Sabbagh, L.D. Sabbagh, IEEE Trans. Magn. **25**, 2646 (1989)
4. I. Dufour, D. Placko, IEEE Trans. Magn. **32**, 348 (1996)
5. D. Placko, N. Liebeaux, *Modèle à sources magnétiques réparties: un concept pour le calcul du champ émis par les dispositifs comportant un circuit magnétique ouvert*, Instrumentation, pour les mesures physiques C2I 2001 (Hermès Sciences Publications 2001, Paris), Vol. 1, ISBN 2-7462-0208-5
6. D. Placko, T. Kundu, Theoretical study of magnetic and ultrasonic sensors: dependance of magnetic potential and acoustic pressure on the sensor geometry, *NDE01 For Health Monitoring and Diagnostic [4335-08], 4–8 mars 2001, Newport Beach, Californie, USA*
7. ANSYS Inc., *ANSYS 6.0 Online Help*, copyright 2002